Science of Sintering, **53** (2021) 285-299

https://doi.org/10.2298/SOS2103285K

UDK: 546.824; 666.651; 667.61; 548.736

Point Defects and their Effect on Dielectric Permittivity in Strontium Titanate Ceramics

Darko Kosanović, Jelena Živojinović, Jelena Vujančević, Adriana Peleš, Vladimir A. Blagojević*)

Institute of Technical Sciences of the Serbian Academy of Sciences and Arts, Knez Mihailova 35/IV, Belgrade, 11000, Serbia

Abstract:

The origin of dielectric properties of strontium titanate ceramics is investigated using DFT calculations in periodic system. It was determined that the main factors contributing to the increase in dielectric permittivity are: tetragonal distortion of the normally cubic lattice, and charge imbalance induced displacement of titanium center from its central position. Oxygen vacancies were determined to create significantly larger effects than other types of vacancies, like Ti and SrO. The extent of tetragonal distortion was found to be determined by oxygen vacancy distribution, rather than total concentration: relatively symmetrical distribution of oxygen vacancies resulted in smaller tetragonal distortion of the lattice, and, consequently, smaller increase in dielectric permittivity. Charge imbalance naturally destabilizes the cubic lattice, forcing the Ti-atom out of its central position, resulting in tetragonal lattice with increased dielectric permittivity. The process stabilizes the strontium titanate lattice, while increasing the c/a ratio. Therefore, the dielectric permittivity of strontium titanate can be increased by changes to the system that increase tetragonal distortion of the lattice and/or introduce additional negative charge.

Keywords*: Strontium titanate; Dielectric properties; Point defects; DFT calculations; Lattice distortion.*

1. Introduction

Strontium titanate ($SrTiO_3$) ceramics represents an important class of technological materials, both as pure $SrTiO_3$ or as a part of a multi-component system [1-7]. This typically requires high-temperature processing of the powder material, resulting in a material that is compact and suitable for further fabrication [8-10]. Strontium-titanate-based materials have been used in a wide range of applications like sensors [11], catalysis [12], UV detectors [13], solar cell [14], multilayer ceramic capacitors (MLCCs) [15], and NOx photocatalysis [16, 17]. Various technological applications of $SrTiO_3$ ceramics are affected greatly by defect diffusion and defect structure [18-20]. In particular, oxygen deficiency gives rise to electrical conductivity, while operations of resistive memory devices involving $SrTiO_3$ includes point and cluster defect diffusion over short time scales. Therefore, doping and defect engineering is of vital importance to performance of low carrier concentration oxide materials like $SrTiO_3$ [21], making this a focus of a number of studies in recent years. Ti defects have stable polar configurations along [100] and [110] directions and have been proposed as the origin of ferroelectricity observed in Sr-deficient $SrTiO_3$ thin films [22, 23]. On the other hand, SrO

*) **Corresponding author:** vladab64@gmail.com

defects have been predicted to have the lowest energy configuration of any point defect in $SrTiO_3$ [24]. However, the most widely studied defect in $SrTiO_3$ has been oxygen vacancies, which induce conductivity in $SrTiO_3$ at carrier density of 10^{19} cm^{-3} [25].

Wang et al. reported giant permittivity and very low dielectric loss in $SrTiO_3$ ceramics sintered in nitrogen, which can be attributed to fully ionized oxygen vacancies and giant defect-dipoles [26]. When further sintered in air, the materials exhibit large temperature- and frequency-dependent dielectric loss, due to the ionization and motion of oxygen vacancies. Local reversible structural changes caused by the application of the external electric field were observed in STO single crystals and attributed to oxygen redistribution. The structural changes involved expansion of the unit cell and a transition from centrosymmetric to a lower symmetry phase due to tetragonal distortion of around 0.005 Å along *c*-axis (*c*/*a* ratio of 1.0012) [27]. A study of the structural and electronic properties of the neutral and positively charged oxygen vacancies in the bulk and on the (001) surfaces of $SrTiO_3$ crystal showed that charged vacancy centers exhibit a stronger local lattice relaxation and significantly deeper energy levels, both in bulk and on the surfaces, as compared with the neutral centers [28]. Cai et al. reported a metal-to-semiconductor transition with varying oxygen content, where metallic state was achieved at oxygen content of 2.63 (x = 2.63 in $SrTiO_x$; or 12.1 % oxygen vacancies) [29]. Strontium titanate also exhibits persistent photoconductivity, which can be attributed to the excitation of an electron from a titanium vacancy defect into the conduction band, with a very low recapture rate [30]. Subjecting $SrTiO_3$ single crystals to strong external electric field causes distortion of the cubic structure and establishes a polar phase due to field-induced redistribution of oxygen vacancies in $SrTiO_3$ and a formation of an inherent dipole moment [31]. This results in a dielectric to pyroelectric phase transition and lattice distortion is field-dependent [27].

Plain-wave *ab initio* calculations of vacancy defects in strontium titanate at two oxygen vacancy concentrations identified defect states within the band gap and determined that the electrons left behind by oxygen removal localized on Sr(Ti)3d orbitals and vacancy sites [32]. Optical properties of cubic $SrTiO_3$ calculated within generalized gradient approximation (GGA) have shown good agreement with experimental data in a wide energy range of 0-32 eV [33].

Herein, we report the dependence of optical properties of $SrTiO_3$ on type and concentration of lattice defects calculated using DFT calculations within GGA and GGA+U methods. In particular, investigation of the dependence of dielectric permittivity on oxygen vacancy concentration shows strong correlation between the extent of tetragonal distortion of the cubic lattice of $SrTiO_3$ and the calculated values of dielectric permittivity. In addition, through comparison of GGA calculations with and without Hubbard U, it is shown that these effects are largely independent on the methodology. It is also shown that excess negative charge in $SrTiO_3$ causes the displacement of Ti-atom from the central position in the lattice, stabilizing the lattice, while reducing the calculated dielectric permittivity at the same time, indicating that both the lattice distortion and the dielectric permittivity in $SrTiO_3$ structure with defects are ultimately caused by the existence of excess charge in the system.

2. Computational Details

DFT calculations on a periodic system were conducted on a unit lattice using ABINIT 8.10 software package [34] with GGA functional [35, 36] with and without Hubbard U [37] and Optimized Norm-Conserving Vanderbilt Pseudopotential ONCVPSP-3.2.3.1 pseudopotential [38]. Energy cutoff was 990 eV and SCF tolerance was $5 \cdot 10^{-7}$ eV per atom.

3. Results and Discussion

In order to examine the effect of different types of point defects on electronic and dielectric properties of strontium titanate ($SrTiO_3$), a series of calculations on 3x3x3 supercell were performed, incorporating four types of defects: oxygen-, Sr-, Ti- and SrO-vacancies. Calculations with oxygen vacancies were performed at different concentrations, due to the fact that point defects tend to cluster in non-stoichiometric $SrTiO_3$, resulting in creation of localized TiO_2 and SrO islands in Sr- and Ti-poor strontium titanate systems, respectively [39-42]. This clustering effect means that a strontium titanate system can contain high local concentrations of oxygen vacancies.

Oxygen vacancies

Table I shows the overview of the results of GGA+U calculations for systems with oxygen vacancies. Geometries were optimized for more than one configuration with the same concentration of vacancies to see the effects of vacancy distribution on electronic structure and dielectric properties of the system. The results show that while there is little effect of vacancy distribution on the width of the band gap, there are significant differences in calculated values of dielectric permittivity in systems with the same concentration of oxygen vacancies. The most stable systems were the ones exhibiting the highest degree of tetragonal distortion and there is a significant increase in the value of the band gap with increase in the concentration of oxygen vacancies.

Tab. I Overview of results of GGA+U calculations on systems with oxygen vacancies.

System	Oxygen vacancy conc.	Eg (eV)	a (Å)	c (Å)	c/a	Tetragonal distortion (%)	ε'	ε''
cubic	0 %	3.23	3.8826	3.8826	1.0000	0.000	4.0	0.0
cubic	1.2 %	3.50	3.8278	3.8288	1.0003	0.028	388.2	155.6
cubic	2.4 %	3.89	3.8300	3.8308	1.0002	0.021	330.9	131.7
cubic	2.4 %	3.89	3.8480	3.8530	1.0013	0.129	926.0	373.2
cubic	2.4 %	3.89	3.8481	3.8527	1.0012	0.118	995.8	401.5
cubic	3.7 %	4.08	3.8521	3.8536	1.0004	0.039	139.8	54.0
cubic	3.7 %	4.08	3.8597	3.8597	1.0000	0.000	14.4	4.7
tetragonal	0 %	3.22	5.4905	7.7647	1.4142	-	4.0	0.0

Fig. 1 shows calculated electron and spin densities in two systems with same concentration but different distribution of oxygen vacancies, exhibiting significantly different values of dielectric permittivity. The system with lower dielectric permittivity is less stable and exhibits more localized electron density, with about 3 % higher maximum values, and higher spin density. This indicates that charge delocalization stabilizes the system and can be correlated with slightly larger lattice and higher degree of tetragonal distortion. The changes in value of the band gap with increase in concentration of oxygen vacancies are inconsistent with experimental results [43, 44], where a slight decrease in value was observed. This deviation from the experimental trend can be attributed to the use of Hubbard U on oxygen atoms: Table II shows that the removal of Hubbard U from the calculation results in a significantly different trend of change in the calculated values of the band gap with increase in the concentration of oxygen vacancies, resulting in more consistency with experimental observations. In addition, it can also be observed that systems optimized with Hubbard U exhibit lower values of lattice parameters and, consequently, lower unit cell volume, even in

the stoichiometric $SrTiO_3$ system. As a result, the calculated values of tetragonal distortion were significantly higher in calculations without Hubbard U.

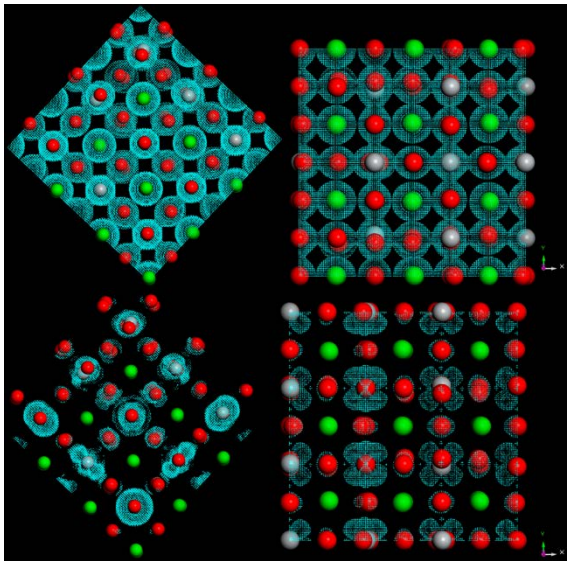

Fig. 1. Electron density (top, isosurface value = 0.6) and spin density (bottom, isosurface value = 0.0005) in two systems with 2.4 % oxygen vacancies with different tetragonal distortions: 0.021 % (left); 0.129 % (right). Green: Sr; Grey: Ti; Red: O.

Tab. II Overview of results of GGA calculations on systems with oxygen vacancies.

System	Oxygen vacancy conc. %	Eg (eV)	a (Å)	c (Å)	c/a	Tetragonal distortion (%)	ε'	ε''
Cubic	0	2.39	3.9053	3.9053	1.0000	0.000	5.7	0.0
Cubic	1.2	2.26	3.8985	3.9013	1.0007	0.072	4.3	0.9
Cubic	2.4	2.22	3.8883	3.9107	1.0058	0.573	227.3	91.9
Cubic	3.7	2.34	3.9097	3.9097	1.0000	0.000	14.4	4.7
cubic	4.9	2.34	3.9054	3.9113	1.0015	0.151	6.7	1.5
cubic	6.2	2.48	3.8612	3.8820	1.0054	0.539	144.1	56.8
cubic*	1.2	2.47	3.8278	3.8288	1.0003	0.028	13.8	3.1
cubic*	2.4	2.50	3.8300	3.8308	1.0002	0.021	15.1	3.6
cubic*	2.4	2.50	3.8480	3.8530	1.0013	0.129	113.3	43.5
cubic*	3.7	2.49	3.8521	3.8536	1.0004	0.039	26.5	8.1

*GGA+U optimized geometry, same as in Table I.

The effect of Hubbard U on the trend of change in the calculated values of the band gap was confirmed by calculating systems with geometries optimized using GGA+U in a single point GGA calculation, as the increase in the value of the band gap with increased concentration of oxygen vacancies was no longer observed.

Fig. 2 shows that there is no significant difference in calculated electron density for the same geometry using GGA+U and GGA, respectively, suggesting that the application of Hubbard U does not affect charge distribution in any significant way. Considering the effect of Hubbard U on band gap, changes in the electronic structure of non-stoichiometric $SrTiO_3$ with increase in concentration of oxygen vacancies are discussed further only in the context of GGA calculations.

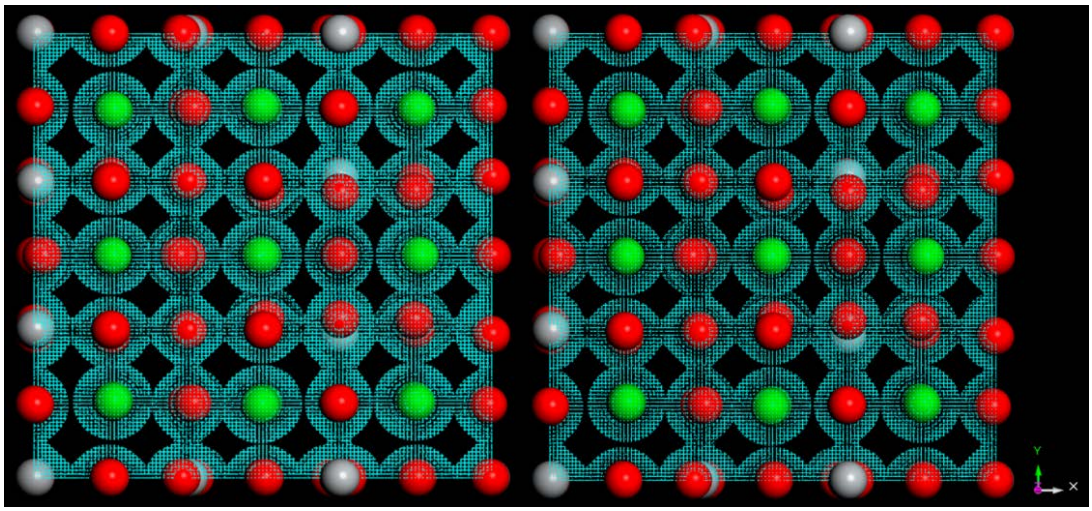

Fig. 2. Comparison of electron densities in the system with 2.4 % oxygen vacancies calculated with GGA+U (left) and GGA (right). Geometry was optimized using GGA+U.

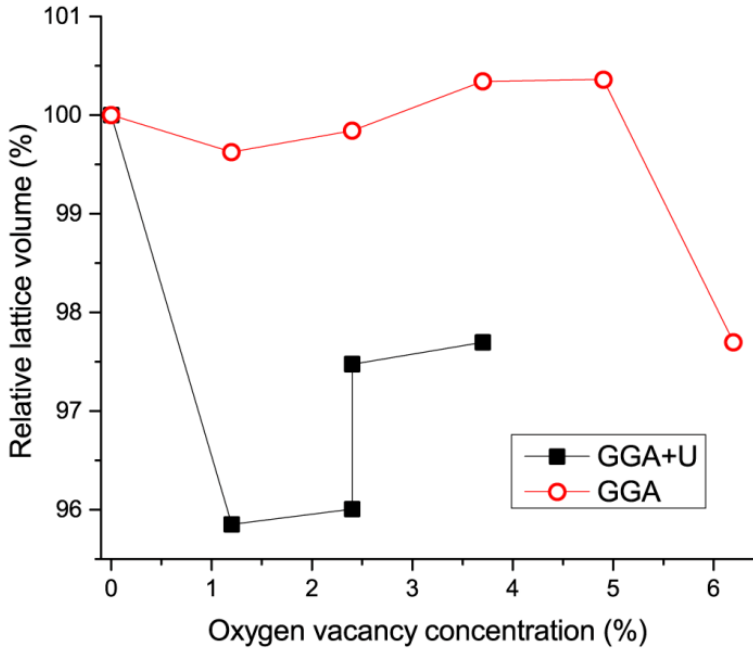

Fig. 3. Relative lattice volume change with change in oxygen vacancy concentration.

Fig. 3 shows the change in relative lattice volume with increase in oxygen vacancy concentration for both GGA+U and GGA calculations. In GGA+U calculations, relatively large changes in lattice volume can be observed even at relatively small oxygen vacancy concentrations. On the other hand, GGA calculations show that relative lattice volume is pretty stable at oxygen vacancy concentrations of below 5 %, where it remains within ± 0.4 % of the volume of stoichiometric $SrTiO_3$. This is in agreement with previous studies: these report that oxygen vacancy produces highly anisotropic elastic dipole tensor, which may provide a mechanism for the vacancy to shield local internal strains. This translates into no observable effects of oxygen vacancy concentration on lattice strain in $SrTiO_3$ systems [45].

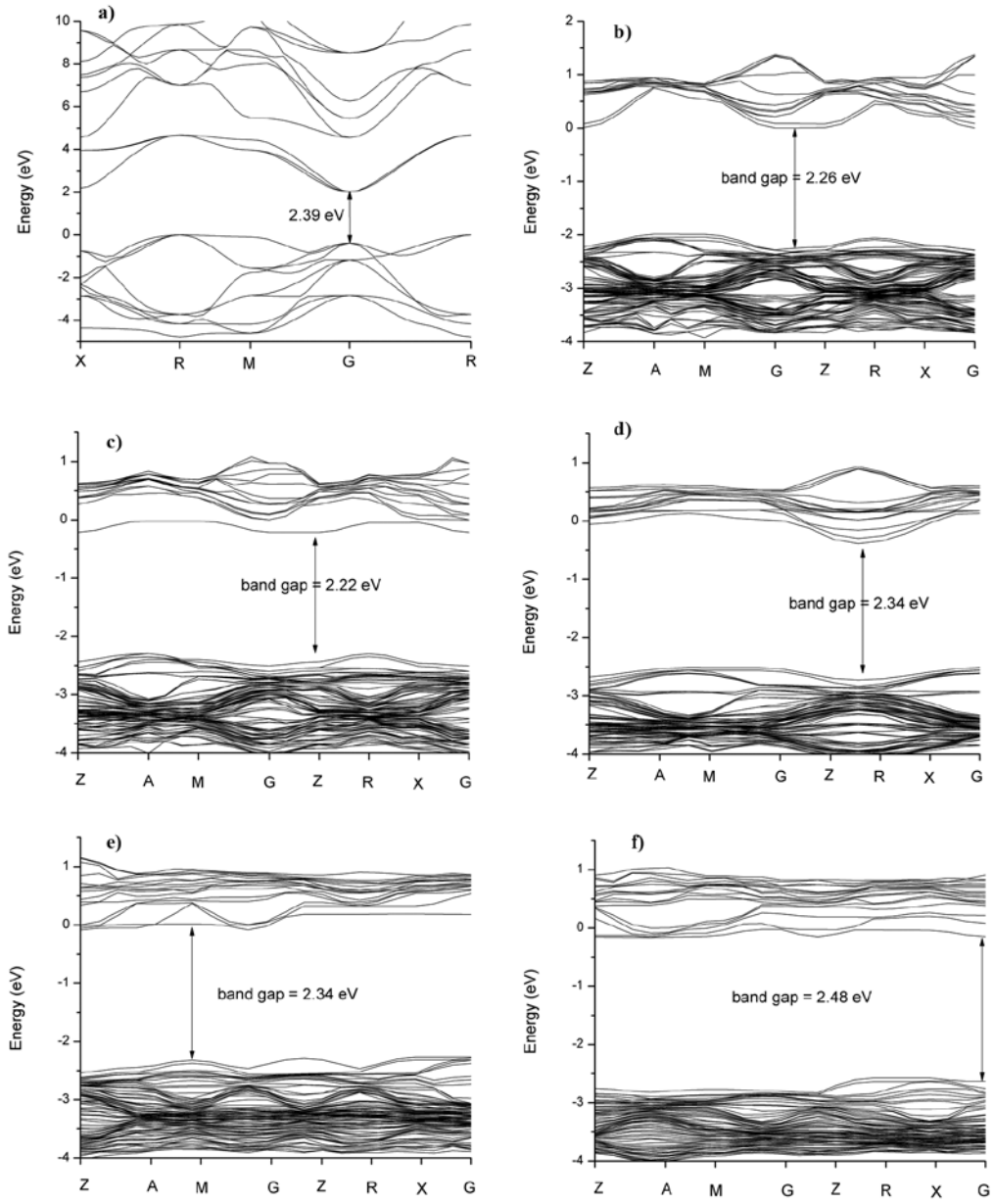

Fig. 4. Band structures of: a) stoichiometric $SrTiO_3$ and non-stoichiometric $SrTiO_3$ with b) 1.2 %; c) 2.4 %; d) 3.7 %; e) 4.9 %; f) 6.2 % oxygen vacancies.

Fig. 4 shows band structure of stoichiometric and non-stoichiometric $SrTiO_3$ with different concentrations of oxygen vacancies calculated using 3x3x3 $SrTiO_3$ supercells. Stoichiometric $SrTiO_3$ exhibits a direct band gap of 2.39 eV at the gamma point, compared to the experimental value of around 3.2 eV. Band structure of non-stoichiometric $SrTiO_3$ suggests that introduction of oxygen vacancies through mechanical activation could result in a small reduction of the band gap, which is consistent with optical properties of mechanically activated $SrTiO_3$ powder [43]. However, introduction of significantly higher concentrations of oxygen vacancies (>2.5 %) into $SrTiO_3$ structure would probably result in expansion of the band gap, as oxygen states in the valence band are eliminated by the process of removal of oxygen atoms from the lattice to create vacancies.

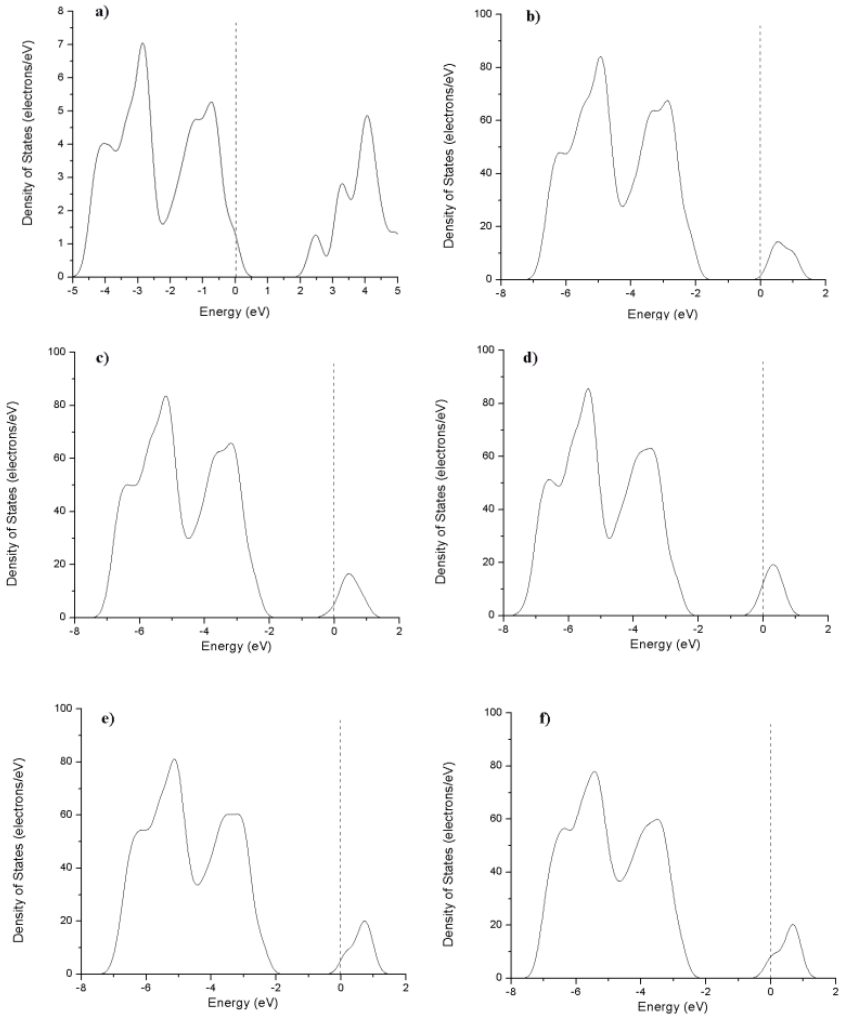

Fig. 5. The calculated density of states for: a) stoichiometric $SrTiO_3$ and non-stoichiometric $SrTiO_3$: b) 1.2 %; c) 2.4 %; d) 3.7 %; e) 4.9 %; f) 6.2 % oxygen vacancies.

Fig. 5 shows the calculated density of states of stoichiometric and non-stoichiometric $SrTiO_3$ 3x3x3 supercells. It can be inferred that the onset of absorption would be fairly sharp, which is consistent with a sharp absorption edge in the optical measurements of mechanically activated non-sintered samples [44]. Fermi level shifts significantly with the introduction of oxygen vacancies, that suggesting non-stoichiometric $SrTiO_3$ lattices would behave like a conductor, rather than a semi-conductor, which is not consistent with experimental results, where non-stoichiometric $SrTiO_3$ does not exhibit electronic conductivity, and can be attributed to the limitations of GGA calculations. However, non-stoichiometric $SrTiO_3$ is known to exhibit ionic conductivity through oxygen ions, where ion mobility is facilitated by oxygen vacancies, allowing oxygen ions to move from one vacant site to another [46, 47]. The introduction of oxygen vacancies also has some effect on the fine structure of the valence band, which is much better defined in stoichiometric $SrTiO_3$, suggesting that the optical absorption spectra of non-stoichiometric $SrTiO_3$ should exhibit somewhat broader peaks. This can be compared to trends observed in the optical measurements of mechanically activated $SrTiO_3$ powder [43], where an increase in the duration of mechanical activation leads to an increase in defect concentration, and the onset of the absorption becomes less sharp at longer activation times.

Other types of vacancies

Other types of vacancies – Ti and SrO, have been shown to have little effect on dielectric permittivity (Table III). This can be correlated with the lack of tetragonal distortion after the introduction of these vacancies. The band gap values are reduced in both cases from the 3.23 eV value of stoichiometric $SrTiO_3$. The decrease is significantly more pronounced for SrO defects, suggesting that the reduction in measured band gap values in experimental system can be associated with the introduction of SrO defects during mechanical activation in addition to oxygen vacancies [43].

Tab. III Overview of results of GGA+U calculations on systems with different types of vacancies.

System	Vacancy type	Eg (eV)	a (Å)	c (Å)	c/a	Tetragonal distortion (%)	ε'	ε''
Cubic	3.7 at.% SrO	1.09	3.9053	3.9053	1.0000	0.000	4.2	0.0
Cubic	3.7 at.% Ti	2.95	3.8751	3.8751	1.0000	0.000	3.5	0.0

Nature of dielectric permittivity

In order to examine the effect of the concentration of the oxygen vacancies on the dielectric properties, DFT calculations were used in a periodic system built around a 3x3x3 supercell with different concentrations of oxygen vacancies. These calculations show that the real part of the dielectric permittivity has maximum value at the concentration of oxygen vacancies of 2.4 % (Fig. 6). The decrease in dielectric permittivity with increase in frequency is consistent with dielectric relaxation in the terahertz region of frequencies. Calculated loss tangent is generally higher in systems with higher values of dielectric permittivity and exhibits an increase with increase in frequency in the terahertz region (Fig. 7), which is consistent with dielectric relaxation in this region. These results are generally consistent with trends observed in experimental measurements of $SrTiO_3$ dielectric materials [48, 49].

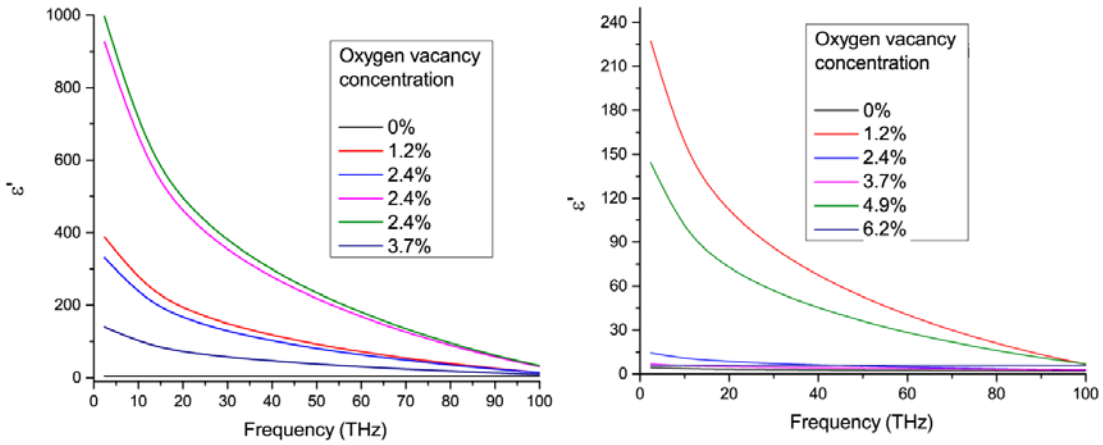

Fig. 6. Dielectric permittivity as a function of frequency for GGA+U (left) and GGA (right) calculations.

DFT calculations have shown that oxygen vacancies represent a major factor in the increase of dielectric permittivity in non-stoichiometric $SrTiO_3$. Other types of vacancies like Sr-, SrO- and Ti-vacancies do not produce the same degree of response, and calculated values of dielectric permittivity in these systems are similar to those of stoichiometric cubic $SrTiO_3$.

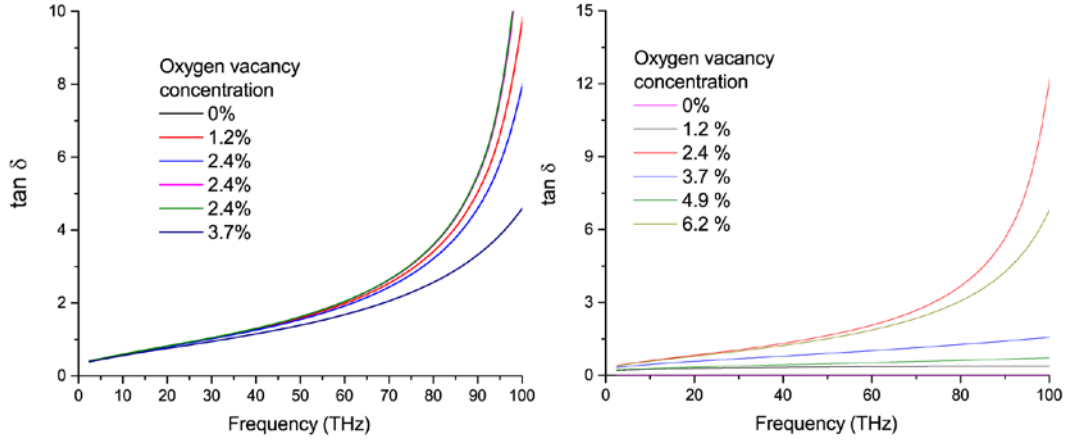

Fig. 7. Loss tangent as a function of frequency for GGA+U (left) and GGA (right) calculations.

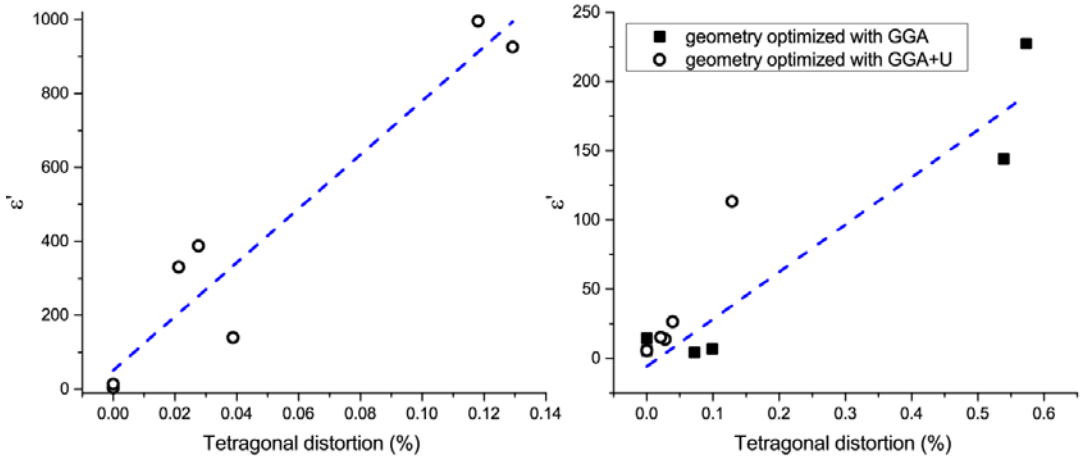

Fig. 8. Correlation of dielectric permittivity (ε') with tetragonal distortion of the lattice in GGA+U (left) and GGA (right) calculations. GGA calculations include two sets of geometries –GGA optimized geometries and GGA+U optimized geometries.

Fig. 8 shows the correlation of dielectric permittivity with the degree of tetragonal distortion in systems with oxygen vacancies for two sets of calculations: one using GGA+U and the other using GGA. GGA calculations were conducted using two sets of geometries: one that was optimized using GGA and the other optimized using GGA+U (which are identical to the geometries used in GGA+U calculations). The comparison of calculations with geometries optimized using GGA+U and calculated using GGA+U and GGA shows that the addition of Hubbard U to the calculation significantly increases the calculated values of dielectric permittivity, and that this increase can be attributed solely to the application of the Hubbard U in the calculation and not to differences in the optimized geometries. Overall, both sets of calculations show that there is a very strong correlation between the value of dielectric permittivity and the degree of tetragonal distortion: the value of R-squared for linear fit is 0.9

for both GGA+U and GGA calculations. This suggests that the degree of tetragonal distortion is a good indicator of the dielectric properties of oxygen-deficient $SrTiO_3$.

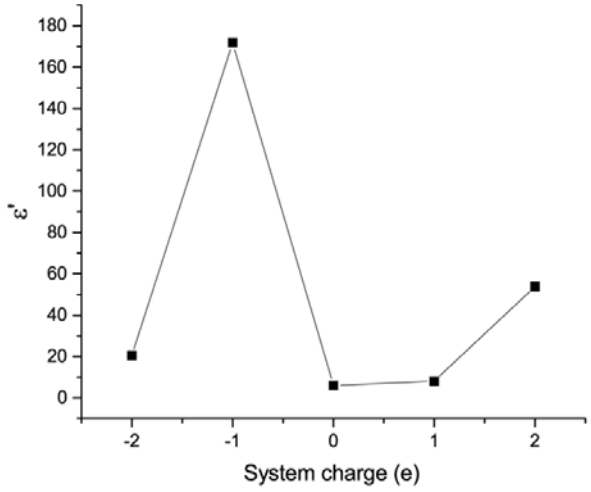

Fig. 9. Dependence of dielectric permittivity on system charge.

In order to investigate the changes in the lattice caused by excess positive and negative charge and the dielectric response of the system in those cases, a series of model systems was constructed incorporating different degrees of tetragonal distortion and different degrees of deviation from normal atomic positions of Sr, Ti and O in the stoichiometric cubic $SrTiO_3$ lattice (Fig. 9). The calculations show that the charge of -1e produces the highest calculated value of dielectric permittivity, while a charge of +1e has a relatively minor effect.

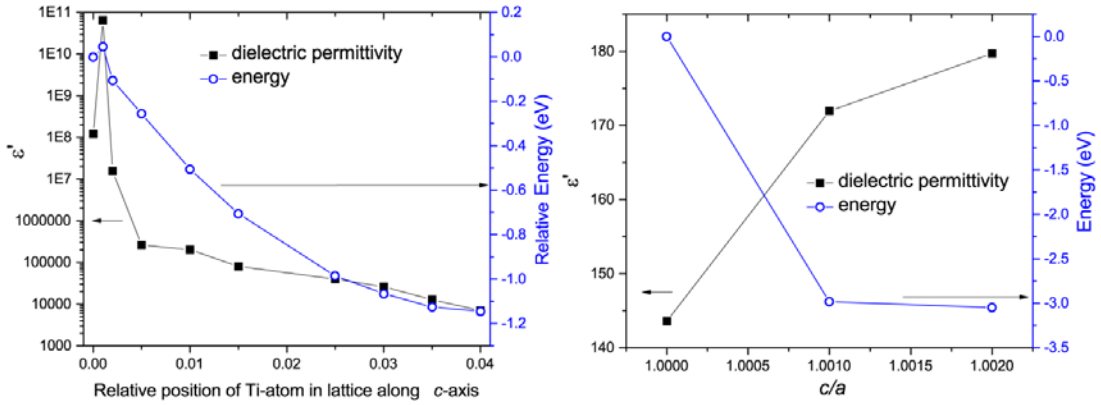

Fig. 10. Change of calculated dielectric permittivity and energy of the system with relative position of Ti-atom along *c*-axis in cubic lattice geometry with a total charge of -1e (left); Change of calculated dielectric permittivity and energy of the system with *c*/*a* with total charge -1e, for Ti-atom relative position of 0.05 (right).

In order to investigate the process of lattice relaxation upon introduction of excess charge and the dependence of dielectric permittivity on structural features of the system, a series of calculations on fixed geometry systems was performed with excess negative charge in the system. Two processes–repositioning of Ti-atom away from the central position and tetragonal deformation of the lattice through elongation along *c*-axis, were considered separately in order to separate the effect of each of these on the dielectric properties and

stability of $SrTiO_3$ system. Fig. 10a shows results of calculations in a fixed cubic lattice with charge of -1e, where Ti was gradually moved along *c*-axis further away from the central position, showing gradual stabilization of the system as Ti was moved further away from its normal site in the cubic lattice. Fig. 10b shows the results of the calculation where the lattice was expanded along *c*-axis, with Ti-atom in a relative position (0, 0, 0.05), indicating that the lattice stabilizes with the introduction of tetragonal distortion. In addition, while the shift of Ti-atom in a charged system reduces the calculated value of the dielectric constant, the tetragonal distortion along *c*-axis leads to an increase.

All these results suggest that when excess negative charge is introduced into $SrTiO_3$, like with creation of oxygen vacancies, the system would most likely respond by breaking the cubic symmetry through a shift in position of Ti-atom and concurrent tetragonal distortion along the *c*-axis. The calculated dielectric permittivity of the system decreases during this stabilization as the system becomes more stable due to increased delocalization of the excess charge, suggesting that delocalization of the excess charge is the main driving force behind structural changes: when excess charge is introduced, the system adapts its structure to delocalize it, minimizing the differences in Coulombic forces in the system.

These results suggest that the effects of point defects on the structure of $SrTiO_3$ ceramics should have longer range effects than their immediate locality: introduction of sufficient concentration of oxygen vacancies should be observable in the disruption of long-range symmetry of the cubic lattice, resulting in tetragonal distortion of $SrTiO_3$ lattice, which should be observable using methods like X-ray diffraction.

4. Conclusion

The investigation of several factors contributing to the dielectric permittivity in strontium titanate ceramics shows that the increase in dielectric permittivity from low values in stoichiometric $SrTiO_3$ is primarily caused by defects in the crystal structure. Of these defects, oxygen vacancies show the greatest effect. However, it was identified that the tetragonal distortion of the cubic lattice of $SrTiO_3$ can be directly correlated with the calculated values of dielectric permittivity. Therefore, any type of defect that results in tetragonal distortion of the lattice should cause an increase in dielectric permittivity of $SrTiO_3$ ceramics. In addition, it was observed that systems with charge imbalance exhibit exceedingly high values of dielectric permittivity in a cubic geometry. However, this geometry is unstable, and the system relaxes by breaking the cubic symmetry through a shift in position of Ti-atom and concurrent tetragonal distortion along the *c*-axis. This relaxation process also results in a decrease of dielectric permittivity. Therefore, two main factors have been identified that can potentially contribute to an increase in dielectric permittivity of $SrTiO_3$ ceramics compared to the stoichiometric system: tetragonal distortion of the cubic lattice caused by defects, and the introduction of charge imbalance in the crystal. This can offer some guidance to the design of $SrTiO_3$-based ceramic materials to achieve higher values of dielectric permittivity.

Acknowledgments

Funds for the realization of this work are provided by the Ministry of Education, Science and Technological Development of the Republic of Serbia, Agreement on realization and financing of scientific research work of the Institute of Technical Sciences of SASA in 2021 (Record number: 451-03-9/2021-14/200175).

5. References

1. J. Han, F. Wan, Z. Zhu, Dielectric response of soft mode in ferroelectric $SrTiO_3$, Appl. Phys. Lett. 90 (2007) 031104.
2. A. A. Sirenko, C. Bernhard, A. Golnik, A. M. Clark, J. Hao, W. Si, X. X. Xi, Soft-mode hardening in $SrTiO_3$ thin films, Nature, 404 (2000) 373-376.
3. P. Kužel, F. Kadlec, H. Nemec, Dielectric tunability of $SrTiO_3$ thin films in the terahertz range, Appl. Phys. Lett. 88 (2006) 102901.
4. A. K. Tagantsev, V. O. Sherman, K. F. Astafiev, J. Venkatesh, N. Setter, Ferroelectric Materials for Microwave Tunable Applications, J. Electroceram, 11 (2003) 5-56.
5. J. W. Liou, B. S. Chiou, Dielectric characteristics of doped $Ba_{1-x}Sr_xTiO_3$ the paraelectric state, Mater. Chem. Phys., 51 (1997) 59-63.
6. Y. J. Wu, Y. H. Huang, N. Wang, J. Li, M. S. Fu, X. M. Chen, Effects of phase constitution and microstructure on energy storage properties of barium strontium titanate ceramics, J. Eur. Ceram. Soc. 37 (2017) 2099-2104
7. D. A. Kosanović, V. A. Blagojević, N. J. Labus, N. B. Tadić, V. B. Pavlović, M. M. Ristić, Effect of Chemical Composition on Microstructural Properties and Sintering Kinetics of (Ba,Sr)TiO_3 Powders, Sci. Sinter. 50 (2018) 29-38
8. W. Rheinheimer, M. Baurer, H. Chien, G. S. Rohrer, C. A. Handwerker, J. E. Blendell, M. J. Hoffmann, The equilibrium crystal shape of strontium titanate and its relationship to the grain boundary plane distribution, Acta Mater. 82 (2015) 32-40.
9. M. Baurer, S. J. Shih, C. Bishop, M. P. Harmer, D. Cockayne, M. J. Hoffmann, "Abnormal grain growth in undoped strontium and barium titanate", Acta Mater. 58 (2010) 290-300.
10. J. Živojinović, V. P. Pavlović, N. J. Labus, V. A. Blagojević, D. A. Kosanović, V. B. Pavlović, Analysis of the Initial-Stage Sintering of Mechanically Activated $SrTiO_3$, Sci. Sinter. 51 (2019) 199-208
11. A. M. Schultz, T. D. Brown, M. P. Buric, S. Lee, K. Gerdes, P. R. Ohodnicki, High temperature fiber-optic evanescent wave hydrogen sensors using La-doped SrTiO3 for SOFC applications, Sens. Actuators, B 221 (2015) 1307-1313.
12. G.-L. He, Y.-H. Zhong, M.-J. Chen, X. Li, Y.-P. Fang, Y.-H. Xu, One-pot hydrothermal synthesis of $SrTiO_3$-reduced graphene oxide composites with enhanced photocatalytic activity for hydrogen production, J. Mol. Catal. A: Chem. 423 (2016) 70-76.
13. F. Jing, D. Zhang, F. Li, J. Zhou, D. Sun, S. Ruan, High performance ultraviolet detector based on $SrTiO_3/TiO_2$ heterostructure fabricated by two steps in situ hydrothermal method, J. Alloys Compd. 650 (2015) 97-101.
14. P. Jayabal, V. Sasirekha, J. Mayandi, K. Jeganathan, V. Ramakrishnan, A facile hydrothermal synthesis of $SrTiO_3$ for dye sensitized solar cell application, J. Alloys Compd. 586 (2014) 456-461.
15. K. Nishida, H. Kishi, H. Funakubo, H. Takeuchi, T. Katoda, T. Yamamoto, Evaluation of Residual Strain and Oxygen Vacancy in Multilayer Ceramic Capacitor Using Laser Raman Spectroscopy, Jpn. J. Appl. Phys. 46 (2007) 7005-7007.
16. L. Chen, S. Zhang, L. Wang, D. Xue, S.Yin, Preparation and photocatalytic properties of strontium titanate powders via sol–gel process, J. Cryst. Growth 311 (2009) 746-748.
17. U. Sulaeman, S. Yin, T. Sato, Solvothermal synthesis of designed nonstoichiometric strontium titanate for efficient visible-light photocatalysis, Appl. Phys. Lett. 97 (2010) 103102.
18. J. Robertson, High dielectric constant gate oxides for metal oxide Si transistors. Rep. Prog. Phys. 69, 2 (2006) 327-396.

19. M. Janousch, G. I. Meijer, U. Staub, B. Delley, S. F. Karg, B. P. Andreasson, Role of oxygen vacancies in Cr-doped $SrTiO_3$ for resistance-change memory. Adv. Mater., 19 (2007) 2232-2235.
20. Marshall M. S. J., Becerra-Toledo A. E., Marks L. D., Castell M. R. (2015) Defects on Strontium Titanate. In: Jupille J., Thornton G. (eds) Defects at Oxide Surfaces. Springer Series in Surface Sciences, vol 58. Springer, Cham
21. E. Ertekin, V. Srinivasan, J. Ravichandran, P. B. Rossen, W. Siemons, A. Majumdar, R. Ramesh, J. C. Grossman, Interplay between intrinsic defects, doping, and free carrier concentration in $SrTiO_3$ thin films, Phys. Rev., B 85 (2012) 195460.
22. Y. Y. Guo, H. M. Liu, D. P. Yu, J.-M. Liu, Ferroelectricity and superparamagnetism in Sr/Ti nonstoichiometric $SrTiO_3$, Phys Rev., B 85 (2012) 104108.
23. H. W. Jang, A. Kumar, S. Denev, M. D. Biegalski, P. Maksymovych, C. W. Bark, C. T. Nelson, C. M. Folkman, S. H. Baek, N. Balke, C. M. Brooks, D. A. Tenne, D. G. Schlom, L. Q. Chen, X. Q. Pan, S. V. Kalinin, V. Gopalan, C. B. Eom, Ferroelectricity in strain-free $SrTiO_3$ thin films, Phys. Rev. Lett., 104 (2010) 197601.
24. M. J. Akhtar, Z. U.N. Akhtar, R. A. Jackson, C. R. A. Catlow, Computer simulation studies of strontium titanate, J. Am. Ceram. Soc., 78 (1995) 421-428.
25. O. N. Tufte, P. W. Chapman, Electron mobility in semiconducting strontium titanate, Phys. Rev. B, 155 (1967) 796-802.
26. Z. Wang, M. Cao, Z. Yao, Q. Zhang, Z. Song, W. Hu, Q. Xu, H. Hao, H. Liu, Z. Yu, Giant permittivity and low dielectric loss of $SrTiO_3$ ceramics sintered in nitrogen atmosphere, J. Eur. Ceram. Soc., 34 (2014) 1755-1760.
27. J. Hanzig, M. Zschornak, F. Hanzig, E. Mehner, H. Stoecker, B. Abendroth, C. Roeder, A. Talkenberger, G. Schreiber, D. Rafaja, S. Gemming, D. C. Meyer, Migration-induced field-stabilized polar phase in strontium titanate single crystals at room temperature, Phys. Rev. B, 88 (2013) 024104.
28. V. E. Alexandrov, E. A. Kotomin, J. Maier, R. A. Evarestov, Eur. Phys. J. B, 72 (2009) 53-57.
29. H. L. Cai, X. S. Wu, J. Gao, Effect of oxygen content on structural and transport properties in $SrTiO_{3-x}$ thin films, Chem. Phys. Lett., 467, 4-6 (2009) 313-317.
30. M. C. Tarun, F. A. Selim, M. D. McCluskey, Persistent Photoconductivity in Strontium Titanate, Phys. Rev. Lett., 111 (2013) 187403.
31. J. Hanzig, E. Mehner, S. Jachalke, F. Hanzig, M. Zschornak, C. Richter, T. Leisegang, H. Stöcker, D. C. Meyer, Dielectric to pyroelectric phase transition induced by defect migration, New J. Phys., 17 (2015) 023036.
32. M. Djermouni, A. Zaoui, S. Kacimi, B. Bouhafs, Vacancy defects in strontium titanate: Ab initio calculation, Comp. Mater. Sci., 49 (2010) 904-909.
33. M.-Q. Cai, Z. Yin, M-S. Zhang, Optical properties of strontium titanate by ab initio calculation within density functional theory, Chem. Phys. Lett., 388 (2004) 223-227.
34. X. Gonze, F. Jollet, F. Abreu Araujo, D. Adams, B. Amadon, T. Applencourt, C. Audouze, J. M. Beuken, J. Bieder, A. Bokhanchuk, E. Bousquet, F. Bruneval, D. Caliste, M. Côté, F. Dahm, F. Da Pieve, M. Delaveau, M. Di Gennaro, B. Dorado, C. Espejo, G. Geneste, L. Genovese, A. Gerossier, M. Giantomassi, Y. Gillet, D. R. Hamann, L. He, G. Jomard, J. Laflamme Janssen, S. Le Roux, A. Levitt, A. Lherbier, F. Liu, I. Lukačević, A. Martin, C. Martins, M. J. T. Oliveira, S. Poncé, Y. Pouillon, T. Rangel, G.M. Rignanese, A.H. Romero, B. Rousseau, O. Rubel, A. A. Shukri, M. Stankovski, M. Torrent, M. J. Van Setten, B. Van Troeye, M. J. Verstraete, D. Waroquiers, J. Wiktor, B. Xu, A. Zhou, J.W. Zwanziger, Recent developments in the ABINIT software package, Comput. Phys. Commun., 205 (2016) 106-131.
35. J. P. Perdew, J. A. Chevary, S. H. Vosko, K. A. Jackson, M. R. Pederson, D. J. Singh, C. Fiolhais, Atoms, molecules, solids, and surfaces: Applications of the generalized

gradient approximation for exchange and correlation. Phys. Rev. B, 46(11) (1992) 6671.
36. A. D. Becke, Density-functional exchange-energy approximation with correct asymptotic behavior. Phys. Rev. A, 38(6) (1988) p.3098.
37. J. Hubbard, Electron correlations in narrow energy bands. Proceedings of the Royal Society of London. Series A. Mathematical and Physical Sciences, 276(1365) (1963) 238-257.
38. D. R. Hamann, Optimized norm-conserving Vanderbilt pseudopotentials. Phys. Rev. B, 88(8) (2013) 085117.
39. D. D. Cuong, B. Lee, K. M. Choi, H.-S. Ahn, S. Han, J. Lee, Oxygen vacancy clustering and electron localization in oxygen-deficient $SrTiO_3$: LDA+U study. Phys. Rev. Lett., 98 (2007) 115503.
40. Y. Tokuda, S. Kobayashi, T. Ohnishi, T. Mizoguchi, N. Shibata, Y. Ikuhara, T. Yamamoto, Strontium vacancy clustering in Ti-excess $SrTiO_3$ thin film. Appl. Phys. Lett., 99 (2011) 033110.
41. Y. S. Kim, J. Kim, S. J. Moon, W. S. Choi, Y. J. Chang, J.-G. Yoon, J. Yu, J.-S. Chung, T. W. Noh, Localized electronic states induced by defects and possible origin of ferroelectricity in strontium titanate thin films, Appl. Phys. Lett., 94 (2009) 202906.
42. D. J. Keeble, R. A. Mackie, W. Egger, B. Löwe, P. Pikart, C. Hugenschmidt, T. J. Jackson, Identification of vacancy defects in a thin film perovskite oxide, Phys. Rev., B 81 (2010) 064102.
43. J. Živojinović, V. P. Pavlović, D. Kosanović, S. Marković, J. Krstić, V. A. Blagojević, V. B. Pavlović, The influence of mechanical activation on structural evolution of nanocrystalline $SrTiO_3$ powders, J. Alloys Compd., 695 (2017) 863-870.
44. H. Trabelsi, M. Bejar, E. Dhahri, M. A. Valente, M. P. Graça, M. Djermouni, A. Zaoui, Evaluation of the relationship between the magnetism and the optical properties in $SrTiO_{3-\delta}$ defective systems: Experimental and theoretical studies, J. Magn. Magn. Mater., 478 (2019) 175-86.
45. D. A. Freedman, D. Roundy, T. A. Arias, Elastic effects of vacancies in strontium titanate: Short- and long-range strain fields, elastic dipole tensors, and chemical strain, Phys. Rev. B, 80 (2009) 064108.
46. K. Szot, W. Speier, R. Carius, U. Zastrow, W. Beyer, Localized metallic conductivity and selfhealing during thermal reduction of $SrTiO_3$, Phys. Rev. Lett., 88 (2002) 075508.
47. S. Menzel, M. Waters, A. Marchewka, U. Böttger, R. Dittmann, R. Waser, Origin of the ultranonlinear switching kinetics in oxide-based resistive switches, Adv. Funct. Mater., 21 (2011) 4487-4492.
48. T. Hoshina, R. Sase, J. Nishiyama, H. Takeda, T. Tsurumi, Effect of oxygen vacancies on intrinsic dielectric permittivity of strontium titanate ceramics, J. Ceram. Soc. Jap. 126 (5) (2018) 263-268.
49. H. Trabelsi, M. Bejar, E. Dhahri, M. Sajieddine, K. Khirouni, P. R. Prezas, B. M. Melo, M. A. Valente, M. P. Graça, Effect of oxygen vacancies on $SrTiO_3$ electrical properties, J. Alloys Compd., 723 (2017) 894-903.

Сажетак: *Порекло диелектричних својстава керамике стронцијум титанат испитано је помоћу ДФТ прорачуна у периодичном систему. Утврђено је да су главни фактори који доприносе порасту диелектричне пермитивности тетрагонална дисторзија кубичне решетке и померање титанијумовог атоме из централног положаја услед небалансираног наелектрисања. Установљено је да кисеоничне ваканције изазивају веће ефекте од других врста ваканција, као што су Ti и SrO.*

Величина тетрагоналне дисторзије је одређена дистрибуцијом кисеоничних ваканција, а не само њиховом концентрацијом: симетрична дистрибуција кисеоничних ваканција је довела до мање тетрагоналне дисторзије решетке, и, последично, мањег повећања диелектричне пермитивности. Додатно наелектрисање дестабилизује кубичну решетку и изазива померање атома титанијума из централног положаја, производећи тетрагоналну решетку са повећаном диелектричном пермитивношћу. Процес дисторзије решетке стабилизује кристалну решетку стронцијум титаната уз повећање a/c. Стога, диелектрична пермитивност стронцијум титаната се може повећати променама које доводе до тетрагоналне дисторзије кристалне решетке и/или уводе додатно негативно наелектрисање.

***Кључне речи**: стронцијум титанат; диелектрична својства; кристални дефекти; ДФТ прорачуни; дисторзија решетке.*